Geophysical Journal International

*Geophys. J. Int.* (2026) **245,** 1–14
Advance Access publication 2026 January 29
Research Paper

https://doi.org/10.1093/gji/ggag038

# Distinguishing water salinity, water saturation and clay content using spectral induced polarization: a tool for monitoring arid soil conditions

V. Iván,[1,2] B. Mary,[3] L. Peruzzo,[2] N. Schwartz,[4] M. Ghinassi[2] and G. Cassiani[2]

[1]*National Institute of Oceanography and Applied Geophysics, Trieste,* 34010*, Italy. E-mail: vivan@ogs.it*
[2]*Department of Geosciences, University of Padua, Padova,* 35131*, Italy*
[3]*Department Tec4Agro, Institute of Agricultural Sciences CSIC, Madrid,* 28006*, Spain*
[4]*Department of Soil and Water Sciences, The Hebrew University of Jerusalem, Rehovot,* 7610001*, Israel*

Accepted 2026 January 7. Received 2025 November 3; in original form 2025 May 28

## SUMMARY

In arid and semi-arid climates, it is critical to assess the state of the soil in terms of water content and water salinity. The use of geophysics, and geoelectrical methods in particular, to this end faces the challenge of discriminating between the effects of water content and pore water salinity on soil electrical resistivity, since these two factors are both inversely related to resistivity. The heterogeneity of soils, with its possible varying clay content, makes the interpretation even more complex. We have investigated the combined effect of water saturation, pore water salinity and clay content using spectral induced polarization (SIP) on controlled laboratory samples. The experiments contribute to the development and application of the SIP method in the area of small-scale data acquisition and processing for hydrogeophysical and environmental purposes. In our experimental setup the above-mentioned three variables were gradually modified under controlled conditions. Ca-montmorillonite and very fine to coarse sand were mixed during multiple dry-wet mixing cycles in order to create artificial soil samples that mimic natural soils. In total, four samples were used with clay content varying from 2 to 8 mass per cent of clay. The other two variables were changed as well: water saturation ranging from 100 per cent to 10 per cent in 9–15 steps, and electrical conductivity of the pore water ranging from 0.05 to 0.7 S $m^{-1}$ in four steps. The statistical analysis of the results indicates that there is a significant positive correlation between quadrature conductivity and the three variables. The obtained data were fitted using a double Cole–Cole model. The analysis of the obtained Cole–Cole parameters along the three variables shows promising results for the separation between the effects of pore water salinity and water content, thus paving the way for fruitful field applications in arid and semi-arid environments.

**Key words:** Electrical properties; Induced polarization; Hydrogeophysics; Hydrology.

## 1 INTRODUCTION

Geoelectrical methods provide diverse toolsets to image the subsurface and monitor its water dynamics through changes in the system's state. These observations might be crucial in arid and semi-arid areas, where the structure and function of agricultural and natural ecosystems are dramatically determined by water availability and its conditions in terms of salinity. An accurate assessment of spatial and temporal soil water distribution may help improve the efficiency of groundwater management and irrigation strategies. Dryland ecosystems can be characterized by heterogeneous soil cover, high salt content in upper soil layers and low levels of soil moisture. Note that also pore water salinity is a crucial parameter in terms of sustainable agriculture and ecosystems.

Since electrical resistivity depends on water saturation, salinity and soil structure, it has been used for the imaging of the unsaturated zone for decades, beginning with Archie's law (G.E. Archie 1942; D.A. Grunat 2013; T. Wunderlich *et al.* 2013). However, understanding the combined effect of soil water content, salinity and soil composition on the electrical signal remains a challenging issue, which often limits the interpretation of the data (D.A. Grunat 2013). The non-invasive mapping of the vadose zone of complex heterogeneous areas, such as arid and

semi-arid regions, may require more convoluted data acquisition and interpretation strategies than what widely used methods such as TDR (Time Domain Reflectometry), GPR (Ground Penetrating Radar) or ERT (Electrical Resistivity Tomography) can provide.

The induced polarization (IP) method is an extended version of the DC (Direct Current) resistivity method, that can be performed either in the time domain or in the frequency domain (A. Kemna *et al.* 2000; L. Slater & D.P. Lesmes 2002; A. Revil *et al.* 2012). IP measurements were historically used mostly for the exploration of metallic ore deposits (D. Jougnot *et al.* 2010), and recently their importance has increased in a wide variety of environmental (P. Kessouri *et al.* 2019) and engineering applications (D.P. Lesmes & S.P. Friedman 2005). Spectral induced polarization (SIP) or frequency-domain induced polarization surveys measure both the resistive and capacitive properties of the subsurface over a large range of frequencies (mHz to kHz). In addition to resistivity, they provide information about the chargeability of the investigated geological materials, which expresses their ability to reversibly store electrical charges (A. Revil *et al.* 2012; Y. Wu & L. Peruzzo 2020; A. Mendieta *et al.* 2021). These conductive and capacitive properties are dependent on textural parameters (e.g. grain and pore size distribution, mineralogical composition and clay content), as well as on electrochemical parameters [e.g. pore fluid composition, surface charge density and cation exchange capacity (CEC) of the porous material] (G. Okay *et al.* 2014).

Other studies demonstrated also the sensitivity of the IP method to water content (C. Ulrich & L. Slater 2004; K. Titov *et al.* 2004; K. Breede *et al.* 2012; T. Kremer *et al.* 2016; A. Revil *et al.* 2023), clay content (G. Okay *et al.* 2014; G. Osterman *et al.* 2019) and salinity (H.J. Vinegar & M.H. Waxman 1984; A. A. Revil & M. Skold 2011; A. Weller & L. Slater 2012; D.A. Grunat 2013; G. Okay *et al.* 2014; L. Peruzzo *et al.* 2018; A. Mendieta *et al.* 2021). Another line of research concluded that IP surveys provide the possibility to discriminate resistivity changes caused by pore fluid variations from those caused by physical properties such as surface area and hydraulic conductivity of the porous medium (A. Kemna *et al.* 2000; L. Slater & D.P. Lesmes 2002; D.A. Grunat 2013). However, well controlled studies that analyse the joint effects of these three variables are scarce, and they are badly needed in order to pave the way for practical field applications.

For this reason, we conducted laboratory SIP measurements on simplified, artificial soils samples (sand–clay mixtures) to observe, under controlled conditions, how the SIP response is affected by water saturation, pore fluid conductivity and clay content, all varied in a systematic manner. The laboratory setup with pre-defined gradients of pore fluid conductivity and saturation levels allowed the performance of measurements with high accuracy. Four samples with clay (Ca-montmorillonite) content of 2, 4, 6 and 8 mass per cent were analysed using saturation fluids of four concentration levels (tap water–NaCl solution with electrical conductivity of 0.05–0.1–0.35–0.7 S $m^{-1}$). The examined saturation range was between 10 and 100 per cent in 9–15 steps.

The aims of the paper are: (1) to create a comprehensive experimental data base regarding the dependence of the SIP signal of sand–clay mixtures on clay content, fluid saturation level and saturating fluid conductivity; (2) to establish relationships between the electrical properties and selected hydrological-chemical properties of unconsolidated deposits or soils and (3) to create the experimental bases for a pedophysical model that can be used for real samples and field applications.

The paper is organized as follows. Section 2 ('Background') provides the theoretical basis of the SIP method and summarizes previous studies focusing on the influence of water saturation, salinity and clay content. Section 3 ('Materials and Methods') describes the preparation of the samples, the experimental setup, the SIP measurement procedure and the data interpretation fitting procedure. Section 4 ('Results') presents and interprets the measured SIP data and fitted parameters in relation to the studied variables. Section 5 ('Discussion') interprets the results and compares the experimental findings with literature results. Finally, Section 6 ('Conclusion and Outlook') summarizes the main outcomes and outlines future applications of the SIP method for monitoring arid soil conditions.

## 2 BACKGROUND

The SIP method involves injecting a sinusoidal electrical current into a porous medium and measuring the resulting phase-delayed electrical potential between an electrode pair at multiple frequencies (in the mHz to kHz range). Based on Ohm's law, the complex impedance of the medium is obtained, which is related to the complex resistivity through a geometric factor. The complex conductivity ($\sigma*$) is the reciprocal of the complex resistivity and can be decomposed into conductivity magnitude ($|\sigma*|$) and phase ($\phi$) or alternatively into in-phase (or real) ($\sigma'$) and quadrature (or imaginary) ($\sigma''$) conductivity components:

$$\sigma* = |\sigma*|\exp(i\phi) = \sigma\prime + i\sigma\prime\prime, \quad (1)$$

where $i$ is the imaginary unit. The in-phase or real conductivity component is related to energy dissipation processes and, thus, provides information about the ability of the material to conduct the flow of electrical charges (D.P. Lesmes & K.M. Frye 2001; A. Revil *et al.* 2012). Meanwhile, the quadrature or imaginary conductivity component is linked to energy storage processes, since it is a result of charge polarization processes occurring, in the given frequency range, predominantly at the mineral–electrolyte interfaces (around the soil particles) (A. Binley & L. Slater 2020). Both components are affected by sample composition (mineralogy, porosity, permeability), pore fluid chemistry, saturation and temperature.

For a further interpretation of the measured electrical spectra, both physical (e.g. P. Leroy *et al.* 2024) and phenomenological models can be used. However, due to the complexity and lack of comprehensive solid theories, phenomenological models are more commonly utilized (L. Slater 2007; A. Mendieta *et al.* 2021). One of the most widely used models is the Cole–Cole model, which describes the complex resistivity in the frequency range of 10 mHz–10 kHz via a four-parameter model (K.S. Cole & R.H. Cole 1941; W.H. Pelton *et al.* 1978; L. Slater 2007; G. Cassiani *et al.* 2009):

$$\rho(\omega) = \rho_0\left[1 - \mathrm{m}\left(1 - \frac{1}{1 + (\mathrm{i}\omega\tau)^{\mathrm{c}}}\right)\right], \quad (2)$$

where $i$ is the imaginary unit, m is the chargeability, $\rho_0$ is the DC resistivity (inverse of the DC electrical conductivity $\sigma_0$), $\tau$ refers to the mean relaxation time associated with the frequency dispersion and c is the Cole–Cole exponent. By modelling the SIP spectrum with such phenomenological relaxation time models, petrophysical information (such as hydraulic conductivity)

can be extracted from the measured data set (G. Osterman *et al.* 2019).

In the following section, we summarize some of the evidence that existing experimental investigations provide concerning the dependence of SIP on the three key variables (water content, pore water conductivity and clay content). As apparent, the collected evidence is complex to summarize, also because of the different experimental approaches adopted in preparing samples, including the nature of the composing material (e.g. type of clay), and in changing the water content and or pore water salinity of the samples during measurements. This testifies even more of the importance of conducting well-controlled experiments on well-conceived sample sets, as we have tried to do in our study.

### 2.1. Studies addressing pore water conductivity and clay content changes

H.J. Vinegar & M.H. Waxman (1984) investigated the induced polarization of fully saturated shaly sand samples of different clay types (kaolinite, illite, chlorite, montmorillonite) and clay contents at different pore water salinities (0.01, 0.1, 0.5, 1.0 and 2.0 M NaCl). They found a non-monotonic dependence between quadrature conductivity and solution conductivity for the shalier samples: a maximum is observable at around 1 S m$^{-1}$ solution conductivity for the sample of 10 per cent clay content, and at around 8 S m$^{-1}$ for the 25 per cent clay content (D.P. Lesmes & S.P. Friedman 2005). However, for 'clean' sandstones (2 per cent clay content), a monotonic increase was observed. Between the clay content and the quadrature conductivity, a strong correlation was observed: $\sigma''$ is generally increasing with clay content.

D.A. Grunat (2013) noted that the quadrature conductivity is weakly dependent on the pore fluid salinity, thus, it might be used to separate between pore water salinity and water content.

G. Okay *et al.* (2014) studied sand–clay (kaolinite and smectite) mixtures with volumetric clay contents of 1 per cent, 5 per cent, 20 per cent and 100 per cent, fully saturated with the following fluids: distilled water, 0.1, 1 and 10 g l$^{-1}$ of NaCl in solution. They found that (1) the in-phase conductivity ($\sigma'$) increases slightly with salinity for higher clay contents, and greatly for the low clay contents of 1 per cent and 5 per cent, while quadrature conductivity ($\sigma''$) is fairly independent of the pore fluid salinity, and shows just slight increase; (2) $\sigma'$ and $\sigma''$ are steadily increased towards the higher clay contents. This is explained by the fact that quadrature conductivity is proportional to the CEC, which is proportional to the clay content.

A. Weller & L. Slater (2012) analysed 67 different samples (sandstones, shaly sandstones and unconsolidated sediments) to examine the relation between pore fluid conductivity varying between 0.0002 and 15 S m$^{-1}$ (at full saturation) and quadrature conductivity. While for many sandstone and unconsolidated sediment samples they found that a power-law relation was applicable, in the case of sand-silt sediments and some of the shaly sandstones a polarization plateau was observable at salinities of 1–5 S m$^{-1}$, which was followed by a decreasing polarization towards the highest salinities.

A. Revil & M. Skold (2011) focused on fully saturated pure sands and sandstones and aimed to describe the salinity dependence of SIP signals based on experimental data and macroscopic models. They concluded that the quadrature conductivity increases with the salinity until 1 S m$^{-1}$, and it becomes independent from it above this value. They noted that their model needs to be completed for clayey sediments and shaly sandstones.

A. Mendieta *et al.* (2021) studied the SIP signal of four types of clay (red and green montmorillonite, illite and kaolinite), saturated at five different NaCl salinity levels (from de-ionized water to 10 S m$^{-1}$ conductivity). The in-phase conductivity increased with salinity for all types of clay, while the quadrature conductivity showed a non-monotonous behaviour: a peak is observable at the 1 S m$^{-1}$ salinity level for the montmorillonite samples and at the 0.1 S m$^{-1}$ salinity level for the other clays. The phenomenon is explained as at a clay-specific threshold of salinity some polarization mechanisms (possibly membrane polarization) stop to act, which causes the decrease of quadrature conductivity.

T. Kremer *et al.* (2016) analysed sand samples fully saturated with water of three different electrical conductivity levels (0.015–0.04–0.1 S m$^{-1}$, NaCl solutions) in the intermediate frequency range of $10^2$–$10^5$ Hz. They observed that the effective quadrature conductivity (linked to the capacitive properties) is more influenced by the fluid conductivity at the frequency range of $10^2$–$10^5$ Hz (compared to the $10^{-1}$–$10^2$ range) and the relation is direct between them.

D.P. Lesmes & K.M. Frye (2001) examined the complex conductivity of the Berea sandstone saturated with different concentration of NaCl brines ($10^{-3}$ to 1 M). Between $10^{-4}$–$10^{-2}$ Hz and $10^{-2}$–$10^4$ Hz they measured an increase and a decrease, respectively in terms of quadrature conductivities. Between $10^{-3}$ and $10^{-1}$ M NaCl concentrations the quadrature conductivity is increasing as a result of an increase in surface charge density.

G. Osterman *et al.* (2019) studied the hydraulic and geophysical properties of synthetic sand–clay mixtures with 0–1–5–10 mass per cent of kaolinite clay, that were fully saturated with a sodium chloride brine having 0.11 S m$^{-1}$ electrical conductivity. Regarding the relation between the in-phase conductivity and the clay content, they did not observe any strong or consistent trend. However, they found that quadrature conductivity is sensitive both to clay content and to clay distribution. In case of homogeneous clay distribution, the quadrature conductivity increases towards the higher clay contents over the whole frequency range, but especially at frequencies above 100 Hz. If the clay is formed into large large (∼5 mm in diameter), randomly dispersed clusters, geophysical responses become more complex parallel to clay content variations. This is explained by the fact that clay distribution controls the active surface area available for polarization. Note that this study, unlike most of the others here reported, used kaolinite clay, that has a much lower surface charge with respect to illite and montmorillonite, thus the retrieved evidence is not fully consistent with the other studies.

### 2.2. Studies addressing changes in pore fluid saturation

K. Breede *et al.* (2012) analysed sand–clay mixtures with 0–5–10–20 mass per cent clay (kaolinite and illite) content and varying water saturation. They expected and observed measurement errors associated with the electrode contact impedance above 1 kHz. In the frequency range between $10^{-3}$ and 10 Hz the quadrature conductivity presents a clay-content and water-content dependent increase followed by a decrease with a characteristic peak at the frequency of about 0.01 Hz. The normalized total chargeability showed a significant increase parallel

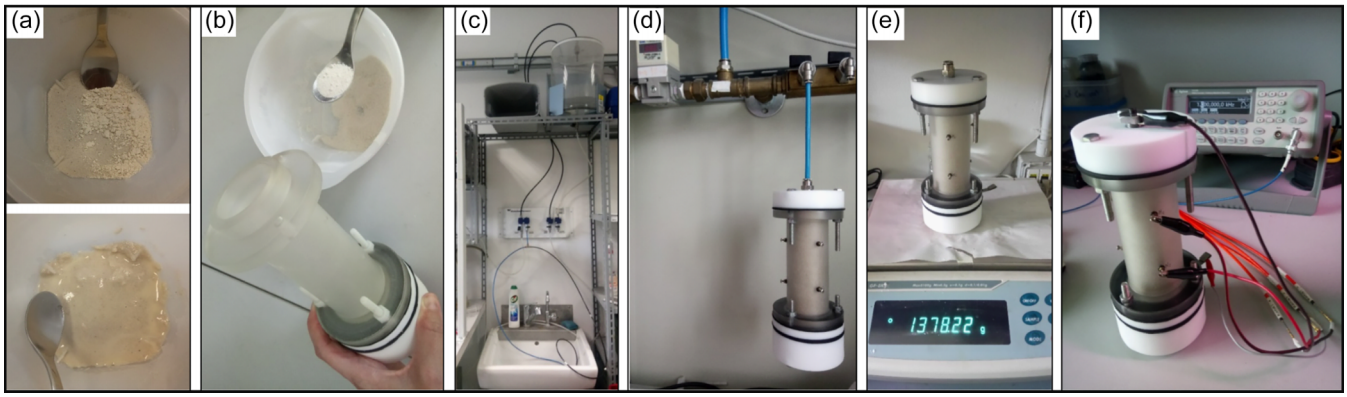


**Figure 1.** Experimental setup: (a) creation of the artificial soil samples. (b) sample packing under dry conditions. (c) saturation of samples. (d) desaturation by air injection. (e) weighing of samples. (f) SIP measurement.

with the clay content, which was explained by the larger specific area of the clays. In case of the higher clay contents (10–20 per cent clay) the chargeability showed monotonous increase with the water saturation, however, for pure sand and 5 per cent clay the change is non-monotonous with a plateau around 60–70 per cent water saturation. The peak of the relaxation time distribution strongly decreases with decreasing water saturation, and the change is more intense towards the higher clay contents.

K. Titov *et al.* (2004) studied quartz sand samples at eight different saturation levels with 100 mg $l^{-1}$ NaCl solution using the Time-Domain IP method. They detected a critical water saturation level in connection with resistivity and chargeability. While the resistivity shows a power-law relationship with the saturation change above this critical saturation, the power-law exponent significantly drops under it. This is explained at the pore scale with the transition of the bulk water into adsorbed water film at the critical saturation.

A. Binley *et al.* (2005) investigated SIP as a function of saturation for sandstone samples. They observed that with decreasing saturation (using saturating fluid of 0.1 S $m^{-1}$ conductivity), the phase peaks are decreasing in amplitude and shifting towards the higher frequencies. The Cole–Cole (CC) model's relaxation time (tau) is decreasing one or two orders of magnitude between saturations of 70 and 25 per cent.

D. Jougnot *et al.* (2010) presented a mechanistic model to interpret SIP data of variably saturated clay-rocks. This model accounts for the polarization of the Stern layer of the electrical double layer and Maxwell–Wagner polarization, and it predicts that the relaxation time is depending just on the dominant diameter of the grains, and not on the sample saturation. However, the experimental results on clay-rocks (20–50 per cent illite, smectite and kaolinite clay matrix with imbedded silica and carbonate grains) showed an increase in relaxation times of about one order of magnitude between 50 and 20 per cent saturation. This was explained by the textural changes of the clay (shrinkage) during desaturation.

C. Ulrich & L. Slater (2004) analysed unconsolidated sediments (mostly sands with negligible clay content) differently saturated with de-ionized water and 0.01 M NaCl solution. They found a power-law dependence between the polarization magnitude and the saturation, with a distinct polarization peak at saturations between 35 and 50 per cent in case of evaporative sample drying, which was absent in case of drainage by air injection under pressure.

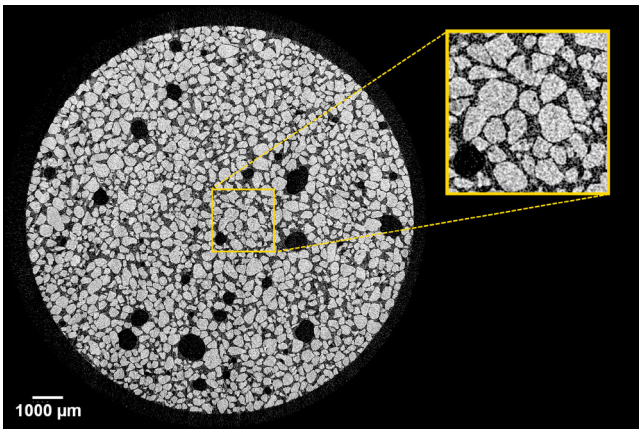


**Figure 2.** Validation of the mixing protocol: MicroCT scan of a small sample (93 per cent of sand, 7 per cent of clay): light grey colour corresponds to the sand, dark to the clay, black to the voids.

## 3 MATERIALS AND METHODS

### 3.1. Sample preparation and measurement setup

In our experiments, the artificial soil samples consisted of very fine-coarse quartz sand ($SiO_2 > 99.6$ per cent, $d = 0.1$–$0.6$ mm, $d_{50} = 0.29$ mm, type 'G20TEAS' from Schlingmeier Quarzsand, Germany) and clay powder (Ca-montmorillonite). For the clay fraction Ca-montmorillonite was chosen because of its electrical and swelling properties. The used Ca-montmorillonite is a source clay from the repository of the Clay Minerals Society, of white colour, and origins from the Manning formation, Jackson group (Eocene) Gonzales County, Texas, USA. Sand and clay were mixed during three dry-wet mixing cycles. One cycle consisted of dry mixing, followed by saturating with tap water (electrical conductivity: 0.05 S $m^{-1}$) and oven drying at 50 °C (Fig. 1a).

The mixing protocol was tested by using an X-ray microCT scan on a small sample with a known clay percentage (7 m per m per cent). The microCT image validated the fact that the microstructure of the artificial mixture imitates sufficiently well natural soils, where the clay is coating the sand grains without larger aggregates (Fig. 2). This is a major difference with respect to the results obtained by using other mixing approaches, as adopted in many previous experimental case studies.

In total, four samples were prepared with gradually increasing clay content of 2, 4, 6 and 8 mass per cent. The samples

were packed into 198 $cm^3$ cylindrical plexiglass cells under dry conditions. The measurement cells were designed to allow the sample saturation and desaturation without significant sample disturbance, as well as the SIP acquisitions in a four-electrode configuration (Fig. 1f), with a design analogous to that used by G. Cassiani *et al.* (2009). The cell caps house the current electrodes (a stainless steel mesh) and tighten the cell through metal screws. The bottom cap encloses a porous ceramic plate that allows water outflow during desaturation via pressurized air injection, while the top cap has the inlet for the saturating water and the pressurized air. The central cell body is equipped with three pairs of stainless steel potential electrodes, each pair positioned 120° apart around the cell axis. The performance of the cell in terms of electrode polarization was tested by filling the cells with tap water, and checking that the resulting phase would be very small as water should lead to zero phase. The performed water test indicates phase values under 1.5 mrad, which is acceptable for the goals of the experiment, as the phase values that are measured and interpreted in the paper are in the 5–50 mrad range (see Supplementary material Fig. S1).

The preparation of unconsolidated samples requires careful attention to detail, since minor differences in column packing can lead to different distributions of mineral–fluid interfaces, and consequently, in the SIP responses (A. Kemna *et al.* 2012). To ensure consistent and homogeneous packing within and between the four samples. The cell body was filled with the dry sand–clay mixture in small portions, each slightly compressed to create an even surface after every three additional spoonfuls (Fig. 1b). The bulk density of the dry samples was in the range of 1.49–1.55 g $cm^{-3}$. Afterwards, the samples were submerged into de-aerated tap water. To ensure full saturation of the cells, they were flushed with a volume of water 2–3 times larger than the cell body volume by applying vacuum (Fig. 1c). The electrical conductivity of the tap water was 0.05 S $m^{-1}$. By weighing the samples, we found that the density of the saturated samples ranged from 1.88 to 1.96 g $cm^{-3}$, with a median of 1.93 g $cm^{-3}$. The porosity of the samples ranged from 0.38 to 0.47, with a median of 0.41. Gradually decreasing saturation was then obtained by air injection with increasing pressure (0.05–2.5 bar) in 9–15 steps (Fig. 1d). The saturation level was determined by weighing the samples at each step, resulting in saturations ranging from 100 per cent to 10–20 per cent (Fig. 1e).

After the first cycle of SIP acquisitions on the four samples, the whole cycle was repeated three additional times for each sample, with increased pore water conductivity. The conductivity was increased by dissolving NaCl in de-aerated tap water, reaching the following levels of electrical conductivity of the solution: 0.1, 0.35 and 0.7 S $m^{-1}$ (at 21°C). The conductivity of the outflow water was measured repeatedly and monitored during desaturation. The advantage of the described procedure is that it allows (1) fairly homogeneous liquid distribution within the sample column, (2) negligible sample disturbance between measurements and (3) constant pore water conductivity during desaturation.

SIP measurements were conducted at each desaturation step using a ZEL-SIP04-V02 impedance meter (Fig. 1f) developed at the Forschungszentrum Jülich (E. Zimmermann *et al.* 2008), at constant 21 (±0.3)°C to avoid temperature effects. A sequence of sinusoidal signals was applied for each frequency, log-spaced in the frequency range from 1 mHz to 45 kHz. A current producing a potential difference of 5 V was applied at the current electrodes and the electrical impedance and phase-shift were measured at the potential electrodes.

### 3.2. Data interpretation

The experiments generated a substantial data set, encompassing approximately 180 measurements. To interpret the SIP results, the measured complex electrical conductivity spectra were analysed using the widely used Cole–Cole model (see eq. 2) (W.H. Pelton *et al.* 1978). The fitting procedure was conducted using the routine developed by M. Weigand & A. Kemna (2016). An example of the Cole–Cole model fitting procedure is provided in the (Supplementary material Fig. S2).

Electromagnetic noise was present at high frequencies essentially due to capacitance effects. This noise can be mitigated by fitting multiple Cole–Cole models to the data—with one model specifically fitted to the high frequencies range to capture the capacitive noise, which is then subtracted from the data set as proposed and applied by W.H. Pelton *et al.* (1978); A. Kemna *et al.* (2000); G. Cassiani *et al.* (2009); K. Breede *et al.* (2012). In this study, a double Cole–Cole model was used, and the high-frequency Cole–Cole component was subtracted from the data in order to analyse only the component linked to the true SIP response. As described in eq. (2), a single Cole–Cole model yield four parameters: the DC resistivity ($\rho_0$), the relaxation time ($\tau$), the chargeability (m) and the Cole–Cole exponent (c).

## 4 RESULTS

The results of the experiments are presented in two steps: first, the raw $\sigma'$ and $\sigma''$ data are shown as a function of saturation, pore fluid conductivity ($\sigma$w) and clay content. This is followed by the analysis of the fitted Cole–Cole parameters across these variables.

In Figs 3, 5 and 8, the complete measured SIP spectra are displayed, while Figs 4, 6 and 7 present a single characteristic $\sigma'$ or $\sigma''$ value at 1 Hz selected to represent the entire spectrum as a function of the controlling variables. The frequency of 1 Hz (or 1.46 Hz) is commonly used for this purpose in unconsolidated samples due to its broad uses in the laboratory, in boreholes and field applications (G. Osterman *et al.* 2019—see also A. Weller & L. Slater 2012; G. Okay *et al.* 2014; A. Mendieta *et al.* 2021).

To compare and interpret saturation-related variations, specific saturation ranges were selected. This approach addressed the limitation that the measurement setup could not achieve exactly the same saturation levels across different samples and measurement repetitions, as the system controls air pressure (and thus suction), not saturation directly. However, covering the 10–100 per cent saturation in 9–15 steps enables to compare over narrow ranges of saturation (3–6 per cent). Thus, to avoid interpolation errors, we chose to keep the measured values rather than interpolating them to the same saturation levels.

### 4.1. Raw SIP results

#### *4.1.1. In-phase conductivity*

The in-phase part of the complex electrical conductivity ($\sigma'$) increases with increasing saturation and is relatively independent

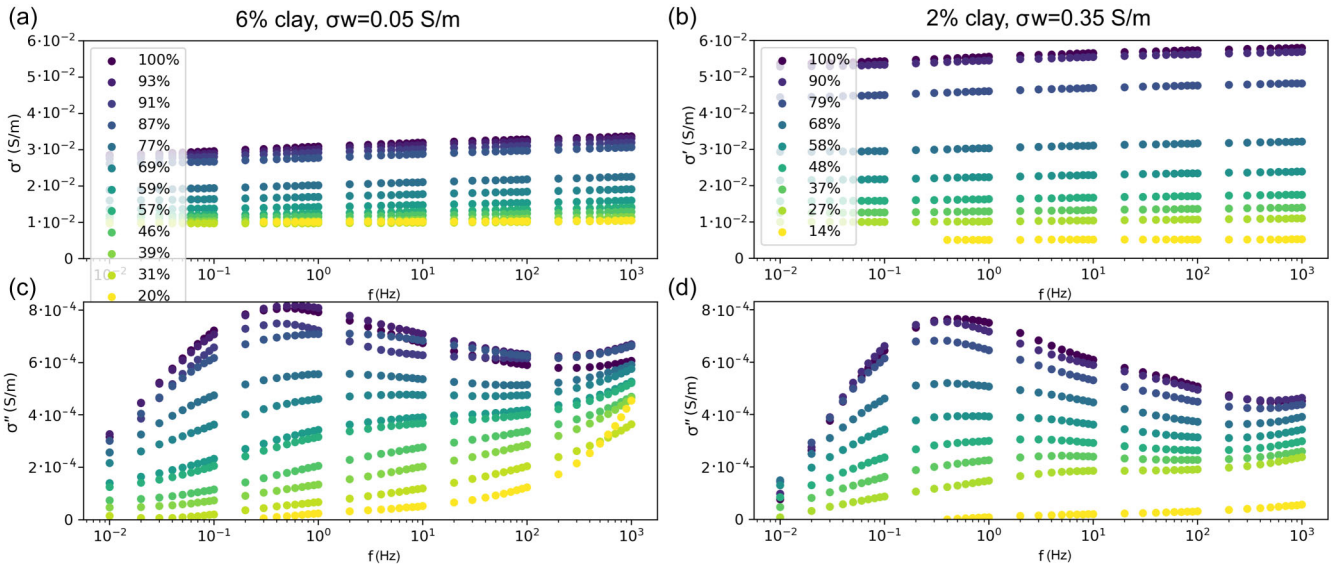


**Figure 3.** In-phase (a and b) and quadrature conductivity (c and d) as a function of frequency and at different water content, illustrated through two examples: (a and c) at 6 per cent clay content, 0.05 S m$^{-1}$ fluid conductivity; (b and d) at 2 per cent clay content, 0.35 S m$^{-1}$ fluid conductivity.

of frequency (only a very subtle monotonic increase is observable towards the higher frequencies), as demonstrated by the results of two examples: 6 per cent clay content at 0.05 S m$^{-1}$ fluid conductivity (Fig. 3a) and 2 per cent clay content at 0.35 S m$^{-1}$ fluid conductivity (Fig. 3b).

Plotting the in-phase conductivity at 1 Hz for the different clay levels as a function of fluid conductivity, we can observe that $\sigma'$ increases with fluid conductivity (Fig. 4). A steeper slope is evident between 0.05 and 0.1 S m$^{-1}$, followed by an approximately linear increase up to 0.7 S m$^{-1}$. In terms of clay contents, a slight increase in $\sigma'$ is detectable towards the higher clay contents at each salinity level. These trends appear to hold true independently of the saturation level (Figs 4a and b).

### 4.1.2. *Quadrature conductivity*

The quadrature conductivity ($\sigma''$) also decreases with decreasing saturation (Figs 3c and d). Between $10^2$ and $10^3$ Hz, an increase is apparent at all saturation levels, which might be due to measurement errors related to electrode contact impedance or other EM effects (D.P. Lesmes & F.D. Morgan 2001; K. Breede *et al.* 2012) (Figs 3c and d). Between $10^{-2}$ and $10^2$ Hz a clear peak is observable at higher saturations. With decreasing saturation, the peak is shifting towards higher frequencies (Figs 3c and d, Figs 5a and c, Figs 8a and c). Another saturation-related observation is that the peak flattens by reaching saturations at around 40 per cent (Figs 3c and d, Fig. 5b, Figs 8b and d), and basically disappears at around 20 per cent saturation level (Figs 3c and d, Fig. 5d).

In Fig. 5, the influence of fluid conductivity ($\sigma$w) on quadrature conductivity is shown using the samples with 2 per cent and 8 per cent clay contents, both for full saturation and lower saturation ranges. The quadrature conductivity increases with increasing salinity at full saturation (Figs 5a and c). However, at lower saturation levels, $\sigma''$ appears to be less dependent on pore fluid conductivity (Figs 5b and d). A similar trend is observed in Fig. 6, where the influence of pore fluid conductivity on quadrature conductivity (at 1 Hz) is presented across the entire saturation range.

Fig. 7 presents the influence of pore fluid conductivity on quadrature conductivity (at 1 Hz) for each clay level at full saturation (Fig. 7a), medium saturation (Fig. 7b) and low saturation range (Fig. 7c). Under full saturation, a rapid increase of the quadrature conductivity occurs between 0.05 and 0.1 S m$^{-1}$, followed by a monotonic increase up until 0.7 S m$^{-1}$ (Fig. 7a). The steep increase between 0.05 and 0.1 S m$^{-1}$ remains characteristic for all clay contents and all saturation levels (Figs 7b and c). However, at lower saturation levels, no clear linear correlation is found between quadrature conductivity and solution conductivity: at medium saturation (44–49 per cent) the dependence is slight and non-monotonic (Fig. 7b), while at low saturation (26–32 per cent) the quadrature conductivity fluctuates in a very narrow range above 0.1 S m$^{-1}$ salinity for all clay contents (Fig. 7c).

Fig. 8 shows the clay content dependence of quadrature conductivity plotted for two pore fluid conductivity levels and two saturation ranges. It is evident that $\sigma''$ increases with increasing clay content at full saturation (Figs 8a and c). Although the trend remains the same at lower saturations between 2–4–6 per cent clay contents (with variation over a narrower range), no significant difference in $\sigma''$ is observed between 6 per cent and 8 per cent clay content (Figs 8b and d).

Based on Fig. 9. we can conclude that the intensity of the increase in quadrature conductivity parallel to saturation is dependent on the clay content: up to approximately 35 per cent saturation level the increase is parallel for all clay levels, and between 6 per cent and 8 per cent clay content just a very slight difference is detected (Figs 8b and d, Fig. 9). Between 35 per cent and 100 per cent saturation levels the increase in $\sigma''$ is significantly more pronounced for higher clay contents (the gradient is significantly steeper towards 8 per cent clay). This observation appears to be independent of the fluid conductivity level (see Fig. 9a and b for 0.05 and 0.35 S m$^{-1}$, respectively). This suggests that low saturation level diminishes the effect of clay content on polarization.

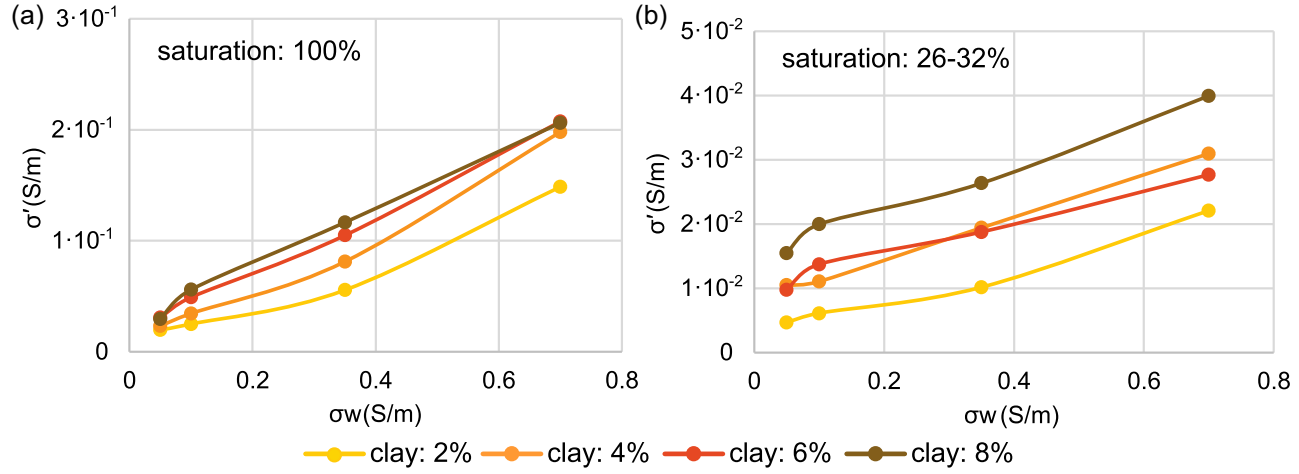


**Figure 4.** In-phase conductivity as a function of salinity and clay content for two saturation ranges: (a) 100 per cent; (b) 26–32 per cent

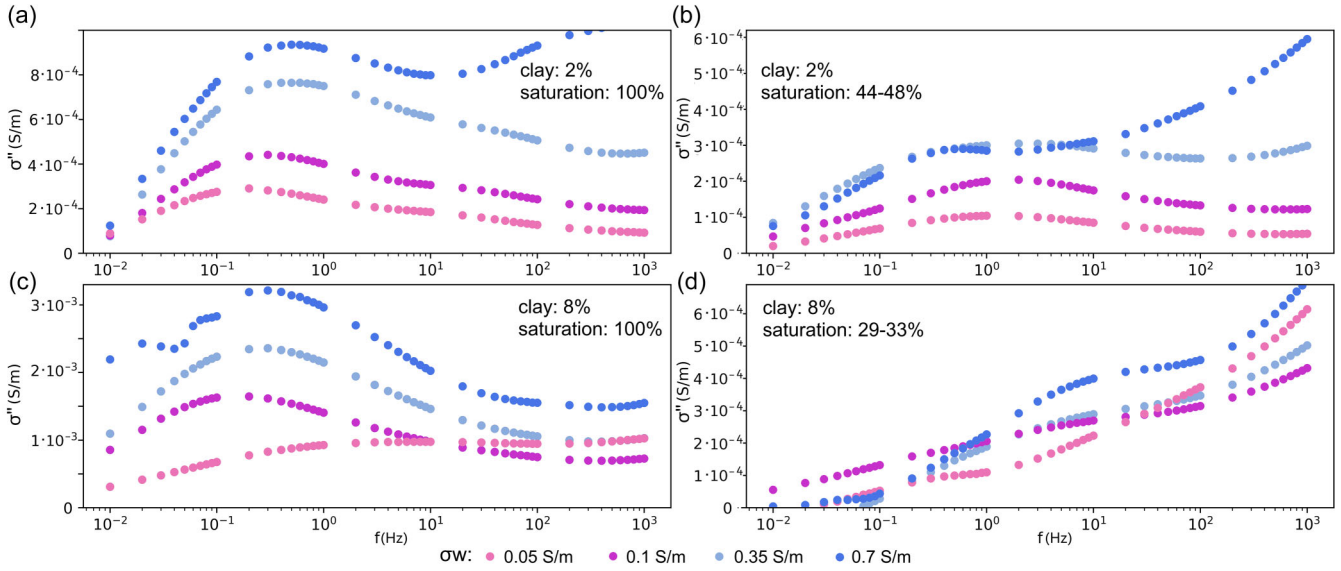


**Figure 5.** Quadrature conductivity as a function of frequency and pore fluid conductivity at (a) 2 per cent clay content and full saturation; (b) 2 per cent clay content and 44–48 per cent saturation; (c) 8 per cent clay content and full saturation; (d) 8 per cent clay content and 29–33 per cent saturation

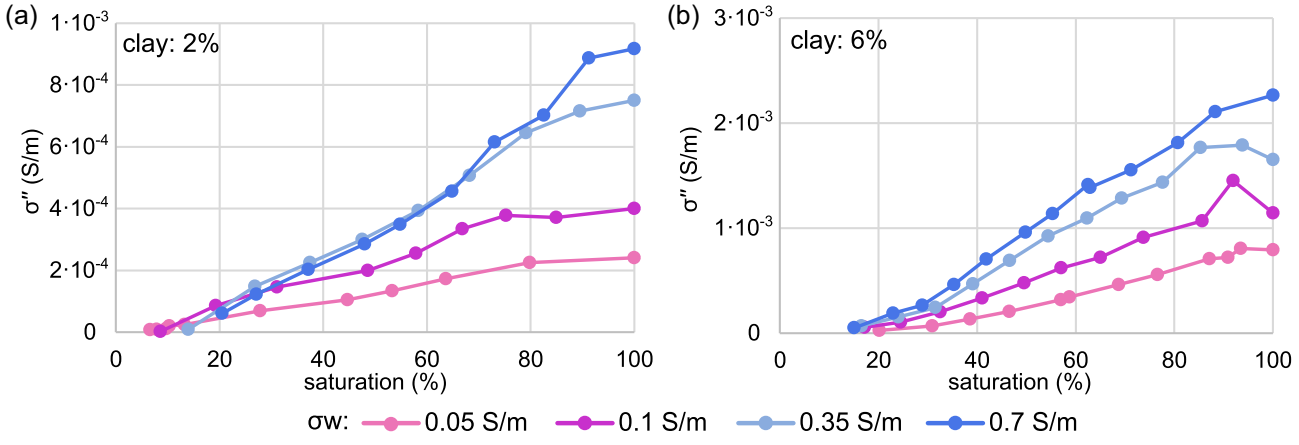


**Figure 6.** Quadrature conductivity (at 1 Hz) as a function of water saturation and pore fluid conductivity at (a) 2 per cent clay content; (b) 6 per cent clay content

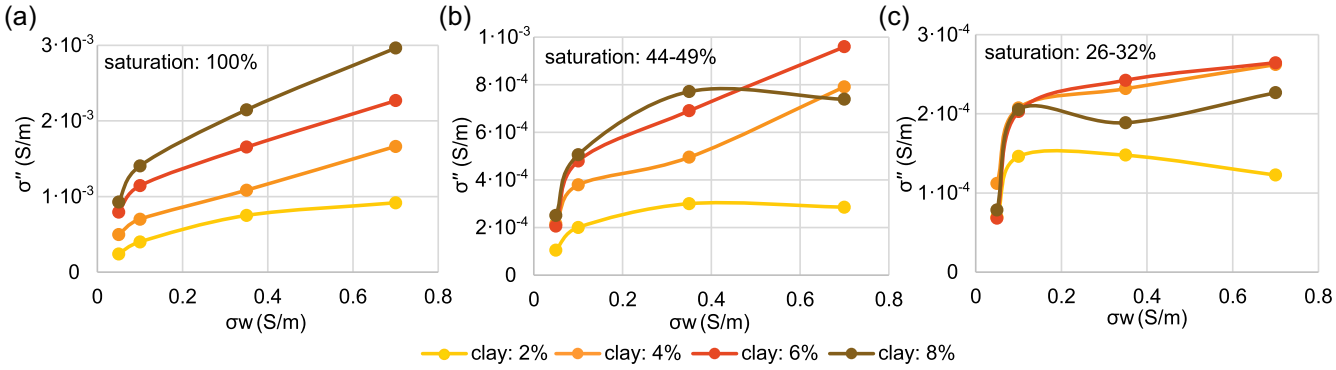


**Figure 7.** Quadrature conductivity (at 1 Hz) as a function of pore water conductivity for all clay levels at (a) full saturation; (b) 44–49 per cent saturation; (c) 26–32 per cent saturation

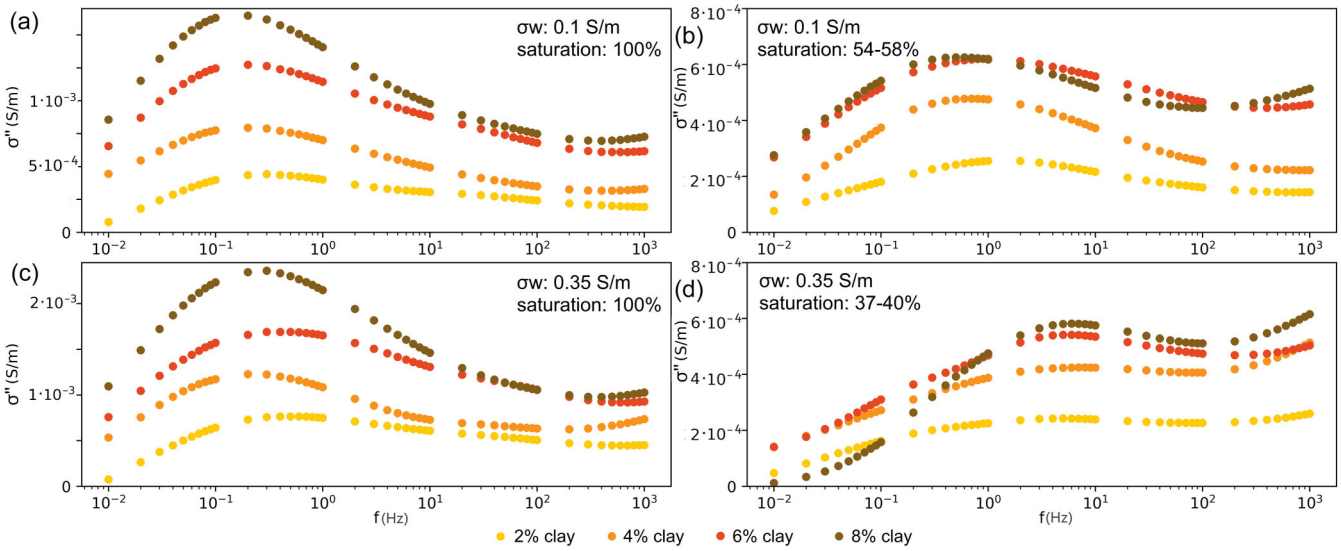


**Figure 8.** Clay content dependence of quadrature conductivity at (a) $\sigma w = 0.1$ S m$^{-1}$ and full saturation; (b) $\sigma w = 0.1$ S m$^{-1}$ and 53–58 per cent saturation; (c) $\sigma w = 0.35$ S m$^{-1}$ and full saturation; (d) $\sigma w = 0.35$ S m$^{-1}$ and 37–41 per cent saturation

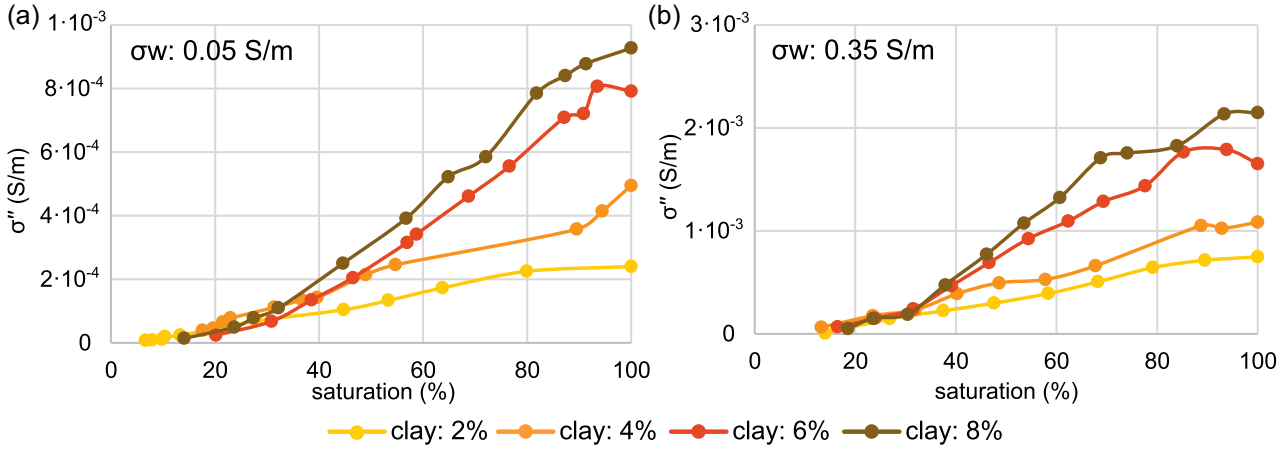


**Figure 9.** Clay content dependence of quadrature conductivity for the whole saturation range (at 1 Hz) on the example of a, $\sigma w = 0.05$ S m$^{-1}$ and b, $\sigma w = 0.35$ S m$^{-1}$

Fig. 10 shows the dependence of the quadrature conductivity (at 1 Hz) on clay content for various fluid conductivity levels across three saturation ranges: 100 per cent, 44–49 per cent and 26–32 per cent (Figs 10a, b and c). At full saturation a linear increase in $\sigma''$ is observable with increasing clay contents for all fluid conductivities levels (Fig. 10a). At medium saturation the linear increase is no longer observed, but a distinct peak in $\sigma''$ appears at 6 per cent clay content for the 0.7 S m$^{-1}$ fluid conductivity (Fig. 10b). At low saturations the non-monotonous relation extends to all fluid conductivity levels: a peak is observed at all fluid conductivities between 4 and 6 per cent clay contents, with a higher peak at larger fluid conductivities.

### 4.2. Fitted Cole–Cole parameters

For a further, more quantitative interpretation of the SIP results, the measured complex electrical conductivity spectra were analysed by applying the Cole–Cole model fitting procedure according to the routine suggested by M. Weigand & A. Kemna (2016) and M. Weigand (2017). The analysis of the Cole–Cole parameters, with special attention to chargeability (m) and mean relaxation time ($\tau$), may help separate the effects of pore water conductivity and water saturation.

Relaxation time (or time constant) $\tau$ is a very important descriptive parameter in the Cole–Cole model, since it directly correlates with the length scale of polarization processes. Its dependence on the grain size has been highlighted, for example, by G. Cassiani *et al.* (2009) and H. Vanhala (1997) or on pore size according, for example, to K. Breede *et al.* (2012). Since the low polarizability at higher saturation levels hinders the proper estimation of relaxation times (K. Breede *et al.* 2012), the analysis of this parameter is restricted to the saturation range of 20–75 per cent (Fig. 11). As fluid saturation decreases, notable trends of decreasing relaxation times emerge. This reduction typically spans a range of 1–1.5 order of magnitude for clay contents of 2–4 per cent, and 1.5–2 orders of magnitudes for clay contents of 6–8 per cent.

Fig. 12 illustrates the chargeability parameter (m) of the Cole–Cole model plotted as a function of saturation. The chargeability shows a non-monotonic relationship with saturation. In most clay contents and fluid conductivity levels, there is a steady increase in chargeability up to 40 per cent saturation, followed by a peak or plateau, and finally a decrease at large saturation levels, with some erratic behaviour near full saturation. In terms of relation to fluid conductivity content, the samples with fluid EC of 0.7 S m$^{-1}$ show the lowest chargeability, while the highest is for the 0.1 S m$^{-1}$ samples. In general, however, the behaviour of chargeability seems to be strongly influenced by data noise, which should be taken into consideration also if chargeability is to be considered as a diagnostic parameter.

## 5 DISCUSSION

We have demonstrated (not surprisingly) that in-phase conductivity ($\sigma'$) decreases with decreasing saturation (Figs 3 and 4), and is relatively frequency-independent: only a subtle monotonic increase occurs in parallel with the increase in frequency (Fig. 3). A slight increase in $\sigma'$ is detectable towards higher clay contents at each salinity level, which can be explained by the large surface area and high CEC of clay minerals, enhancing polarization. This observation is in accordance with the findings of, for example, G. Okay *et al.* (2014). Note, however, that G. Osterman *et al.* (2019) for kaolinite clays did not detect clear connection between these variables. This is explained by the fact that the CEC of kaolinite ranges between 5 and 15 meq per 100 g, while the CEC of montmorillonite ranges between 80 and 150 meq per 100 g. The in-phase conductivity ($\sigma'$) strongly increases with salinity for all clay contents (2–8 per cent) which agrees with the conclusions of G. Okay *et al.* (2014) (up to 5 per cent clay content) and of A. Mendieta *et al.* (2021) (for clean clay samples).

Regarding the quadrature conductivities ($\sigma''$) we demonstrated a positive correlation with saturation changes which is highly dependent on the measuring frequency. At higher saturations a peak is observed between $10^{-2}$ and $10^{2}$ Hz which shifts towards the higher frequencies and flattens at around 40 per cent saturation, then disappears at approximately 20 per cent saturation. The observation is consistent with what would be expected in mixed systems, and it is similar to the observations of K. Breede *et al.* (2012) for sand–clay samples, of C. Ulrich & L. Slater (2004) for unconsolidated sands and of A. Binley *et al.* (2005) for consolidated sands. The cause of this observation lies in the fact that, at lower saturations, the pathways are shorter, thus, the polarization relaxes faster, resulting in peaks at higher frequencies.

The quadrature conductivity ($\sigma$'') is steadily increasing also towards higher clay contents, as long as the saturation is in the range of 35–100 per cent (Fig. 9), consistent with the observations of H.J. Vinegar & M.H. Waxman (1984) and G. Okay *et al.* (2014). The phenomenon can be explained by the fact that, during the saturation process, the added fluid is first trapped by the clay particles, resulting in less polarization. When the saturation level reaches 35 per cent, at lower clay contents the additional liquid will go to the sand, while at higher clay contents it will continue to be added to the clay.

We found that $\sigma$'' is dependent on pore fluid conductivity (showing a positive correlation), which is in accordance with D.A. Grunat (2013) and in disagreement with G. Okay *et al.* (2014), who found these parameters to be fairly independent of each other. This relation is also frequency-dependent (an increase between $10^{-2}$ and $10^{-1}$ Hz followed by a decrease between $10^{-1}$ and $10^{2}$ Hz) which is similar to those described by D.P. Lesmes & K.M. Frye (2001). In contrast, T. Kremer *et al.* (2016) found for sand samples that $\sigma$'' is most strongly influenced by fluid conductivity in the $10^{2}$–$10^{5}$ Hz range (compared to the $10^{-1}$–$10^{2}$ range), which does not seem to hold true in the presence of clay (see Fig. 5).

We also concluded that the quadrature conductivity tends to present a nonlinear, non-monotonous behaviour in relation to fluid conductivity changes (Fig. 7). A. Weller & L. Slater (2012) stated that a polarization plateau was observable at salinities of 1–5 S m$^{-1}$, which was followed by a decreasing polarization towards the highest salinities. In our case the samples at full saturation do not reach this plateau up to the maximum of 0.7 S m$^{-1}$, but at lower saturation levels they show a notable plateau even at lower fluid conductivities (at around 0.35 S m$^{-1}$) in most cases (Figs 7 and 8). A. Revil & M. Skold (2011) also found that $\sigma$'' increases with the fluid conductivity up to 1 S m$^{-1}$, and it becomes independent from fluid conductivity above this value. Our data set does not cover this entire fluid conductivity range, but the presented tendencies may support this general behaviour: between 0.05 and 0.1 S m$^{-1}$ a dramatic increase is observed in

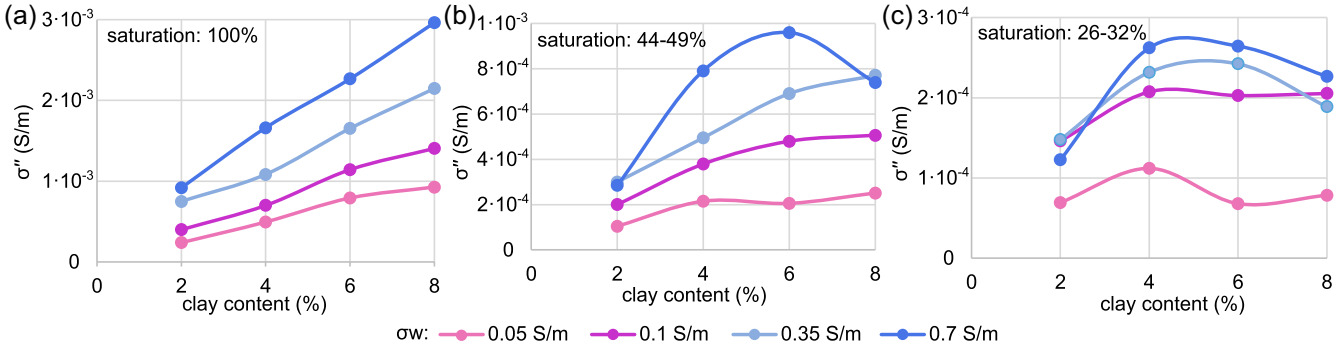


**Figure 10.** Clay content dependence of quadrature conductivity for each fluid conductivity levels at 1 Hz at (a) full saturation; (b) 44–49 per cent saturation; (c) 26–32 per cent saturation.

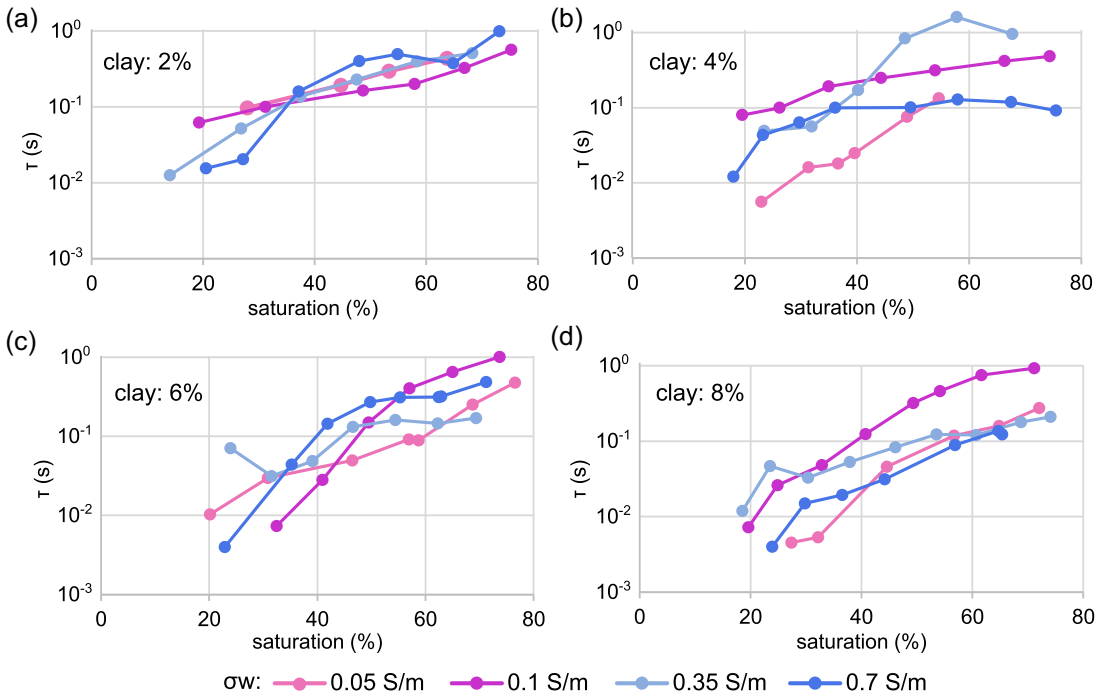


**Figure 11.** Mean relaxation time ($\tau$) obtained from the Cole–Cole model as a function of water saturation for all fluid conductivity levels, for the clay content of (a) 2 per cent; (b) 4 per cent; (c) 6 per cent; (d) 8 per cent.

$\sigma$", and the change is less pronounced between 0.35 and 0.7 S $m^{-1}$. This trend is observed across all clay levels, consistent with the findings of A. Mendieta *et al.* (2021), who described a similar salinity threshold of 1 S $m^{-1}$ for 100 per cent montmorillonite samples (and a lower threshold of 0.1 S $m^{-1}$ for other clays).

In terms of chargeability we found a non-monotonic relationship with saturation changes, reaching a plateau at around 50 per cent saturation (Fig. 12)—a finding that agree with the results of K. Breede *et al.* (2012) and K. Titov *et al.* (2004). This non-monotonic behaviour can be explained as follows: at low saturations, thin water films around mineral surfaces dominate conduction and polarization, so chargeability increases as more water bridges form, enhancing polarization. Around 50 per cent saturation, the system may reach an optimal configuration for polarization (maximum surface area in contact with conductive fluid), causing the peak or plateau. At high saturations, larger water-filled pores short-circuit polarization, reducing chargeability, which explains the decrease at high saturation levels.

Considering the relationship with fluid conductivity, chargeability increases with increasing fluid conductivity up to 0.1 S $m^{-1}$, and decreases after, towards 0.7 S $m^{-1}$ (Fig. 12). An explanation for these trends is that at fluid conductivities from 0.05 to 0.1 S $m^{-1}$, there are more ions available to polarize, which increases chargeability. However, towards 0.7 S $m^{-1}$ fluid conductivity, chargeability decreases because polarization is effectively bypassed: the ions move too easily, reducing charge buildup at interfaces.

The dependence of relaxation time ($\tau$) on fluid saturation changes is often discussed in the literature. We found that $\tau$ shows a clear positive correlation with the saturation (Fig. 11). This trend can be attributed to shortened effective polarization paths as the remaining water forms thinner films or disconnected clusters. This relation is significant for all clay contents,

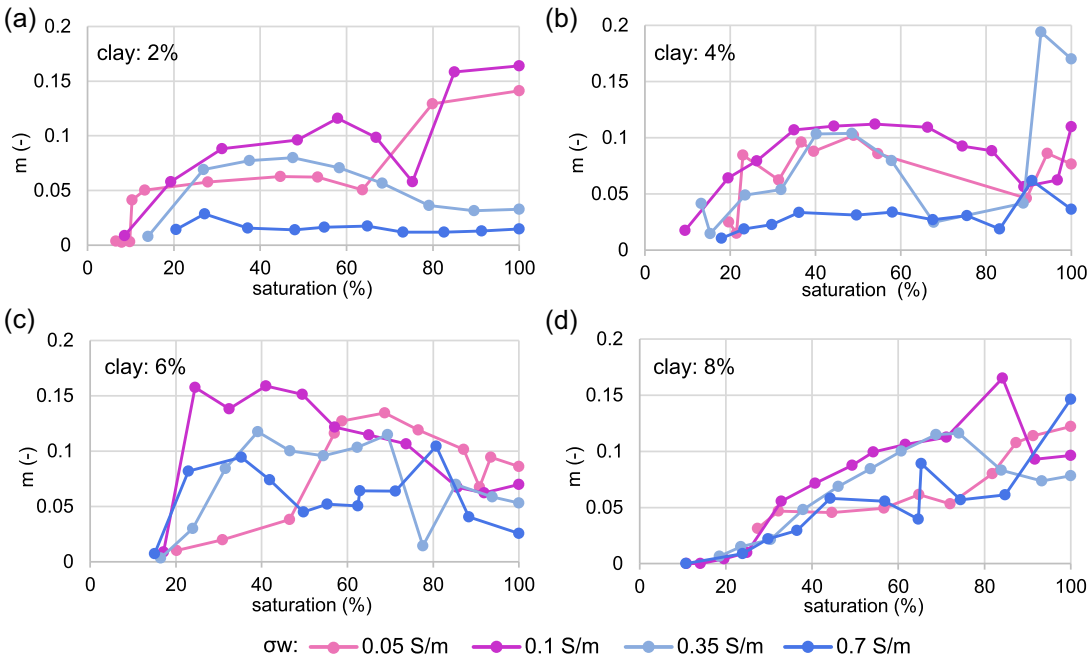


**Figure 12.** Chargeability (m) obtained from the Cole–Cole model as a function of water saturation for all fluid conductivity levels, for the clay content of (a) 2 per cent; (b) 4 per cent; (c) 6 per cent; (d) 8 per cent.

but a stronger dependence on saturation is observed in case of higher clay contents. Our conclusions are in accordance with A. Binley *et al.* (2005) and K. Breede *et al.* (2012) and in disagreement with D. Jougnot *et al.* (2010), who modelled relaxation time as inversely dependent on saturation.

The statistical analysis of the in-phase conductivity, quadrature conductivity and the obtained Cole–Cole parameters confirms the observed sensitivity of the SIP method to water saturation, pore fluid conductivity and clay content (Table 1). The Pearson's correlation coefficients indicate a moderately strong negative correlation between DC resistivity and saturation, and between DC resistivity and pore fluid conductivity; as well as a moderately strong positive correlation between in-phase conductivity and saturation, in-phase conductivity and pore fluid conductivity, quadrature conductivity and saturation, and relaxation time and saturation. Low but significant correlations are observed between quadrature conductivity and pore fluid conductivity, quadrature conductivity and clay content, DC resistivity and clay content, chargeability and saturation, chargeability and pore fluid conductivity, Cole–Cole exponent and saturation, and Cole–Cole exponent and pore fluid conductivity (Table 1). The assumed connection between these parameters might be even stronger in those cases where a non-monotonic relation was described.

A practical use of these results may be derived by comparing the fitted CC parameters of different measurements that resulted in the same resistivity, with the purpose of differentiating between the influence of pore water conductivity and water saturation. An example is presented on Fig. 13, where given a known clay content (4 per cent) we analyse all data sets, that resulted in the same resistivity (39–43 ohm m). As expected, the samples with different pore fluid conductivity levels, reached the same resistivities at different saturation levels (Fig. 13a). The fitted CC model parameters of each measurement reveal further distinctive trends. In our example (Fig. 13), the selected resistivity value was reached at a saturation level of 18 per cent for the sample with pore fluid conductivity of 0.7 S m$^{-1}$ (dark blue dot), which belonged to the lowest values of mean relaxation time ($\tau$) and chargeability (m). In conclusion, by comparing the corresponding fitted CC model parameters of each data set (Fig. 13b), the clear trends (especially for $\tau$ and m) between fluid conductivity levels suggest that the separation between water saturation and pore water conductivity is possible. This possibility for separation is of key importance under field conditions, where from one extensively mappable parameter (resistivity) we can deduce multiple explaining variables with complex spatial patterns, that are only measurable pointwise (e.g. for calibration purposes). The distinguishable CC model parameters behind the same resistivity value enables the mapping of water saturation even in case of changing pore water conductivity.

This observation projects forward the possibility of a future field application, the steps of which are summarized in Fig. 14 from field investigations through laboratory measurements to data processing.

## 6 CONCLUSION AND OUTLOOK

The sensitivity of the SIP method to saturation, clay content and pore fluid conductivity changes has been demonstrated recently by different authors. According to our knowledge though, their combined effect on the SIP signal has not been studied yet. By performing around 180 SIP measurements we obtained and analysed a good experimental data set regarding the dependence of the SIP signal of sand–clay mixtures with the clay content, fluid saturation level and saturating fluid conductivity. The mixtures were prepared in order to make samples where the distribution of clay minerals is realistically mimicking natural samples. This is critical in order to properly account for the presence

**Table 1.** The Pearson's correlation coefficients between the sample variables (saturation, pore fluid conductivity, clay content) and the measured in-phase conductivity ($\sigma'$), quadrature conductivity ($\sigma''$), and the obtained Cole–Cole parameters (DC resistivity ($\rho 0$), chargeability (m), relaxation time ($\tau$), Cole–Cole exponent (c)). Note that for the relaxation time ($\tau$) just the saturation range of 20–75 per cent was considered.

| | Saturation | Pore fluid conductivity | Clay content |
|---|---|---|---|
| $\sigma'$ | 0.57 | 0.65 | 0.16 |
| $\sigma''$ | 0.70 | 0.41 | 0.38 |
| **C0–$\rho$** | − 0.65 | − 0.68 | − 0.33 |
| **C1–m** | 0.36 | − 0.37 | 0.15 |
| **C2–$\tau$** | 0.62 | − 0.03 | − 0.17 |
| **C3–c** | − 0.27 | 0.20 | − 0.04 |

| **Pearson's correlation coefficient ranges** | |
|---|---|
| −0.8 to −0.5 | Moderate negative correlation |
| −0.5 to −0.2 | Low negative correlation |
| −0.2 to 0.2 | Negligible correlation |
| 0.2 to 0.5 | Low positive correlation |
| 0.5 to 0.8 | Moderate positive correlation |

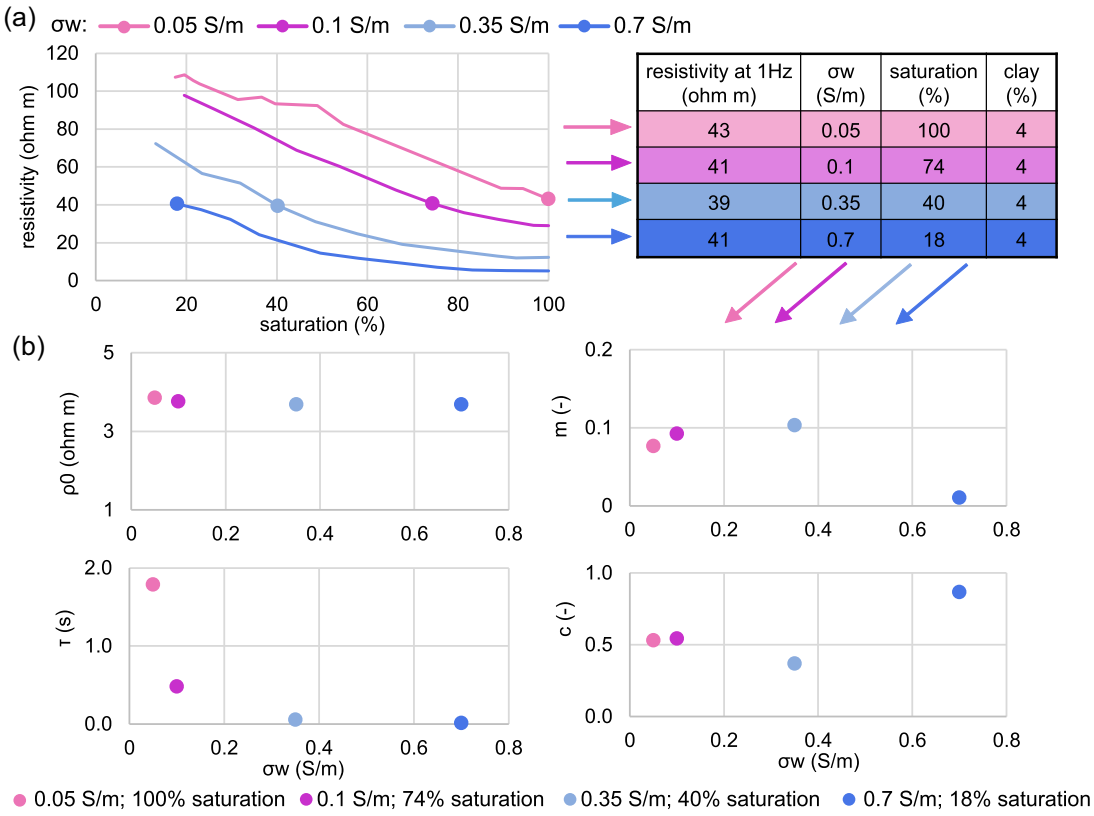


**Figure 13.** Comparison of CC parameters belonging to samples of 39–43 ohm m resistivities and 4 per cent clay content: (a) the selected resistivity range is reached at different saturation by the samples of different pore fluid conductivity levels; (b) CC parameters: DC resistivity ($\rho 0$), chargeability (m), relaxation time ($\tau$), Cole–Cole exponent (c)

of clay and its effect in terms of polarization, and is rarely done in previous studies.

The laboratory experiment demonstrated the sensitivity of the SIP method to water content, clay content and pore fluid conductivity. The statistical analysis of the results indicates that there is a significant positive correlation between quadrature conductivity and these three variables. The measured SIP spectra were further interpreted using a Cole–Cole model which provided chargeability and relaxation time values. Both parameters show significant positive correlation with saturation, while chargeability is negatively correlated with pore fluid conductivity. The connection between the analysed parameters might be even stronger in those cases where a non-monotonic relation was described. These results show a great potential for the separation between pore water conductivity and water content. The analysis of the electrical properties measured with the SIP method reveals that these complex properties are in fact composed of distinct components. This separation is of key importance in complex field settings. Future work will focus on creating a pedophysical model based on the presented experimental bases that can be used for real soil samples and for field applications. The performance of the model will be tested in field sites representing different semi-arid and arid ecological conditions.

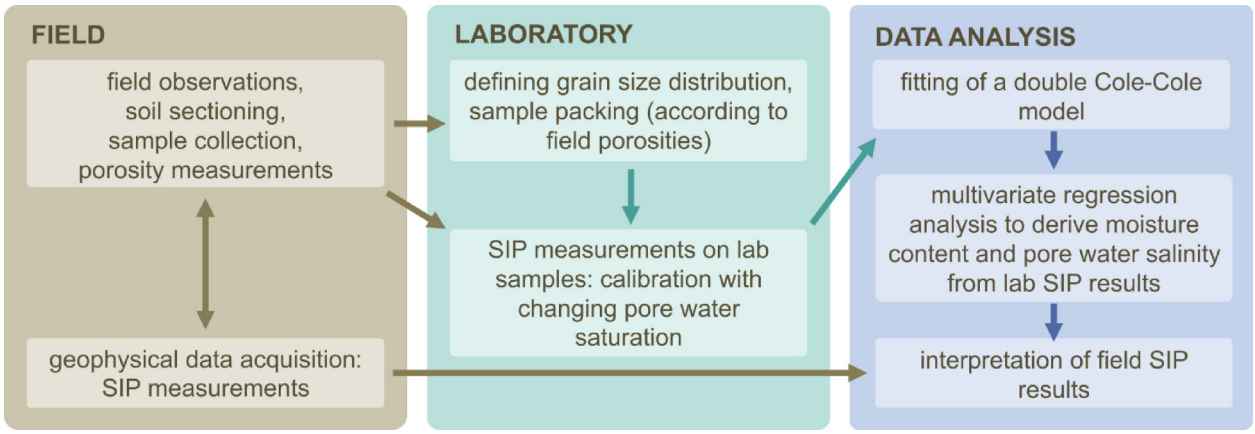


**Figure 14.** Workflow of a practical approach to derive moisture content and pore water salinity, independently, from SIP results

## ACKNOWLEDGMENTS

The authors wish to acknowledge financial support from the EU FP7 ERANET-MED project WASA (WAter Saving in Agriculture: technological developments for the sustainable management of limited water resources in the Mediterranean area); from the project ECZ-Dry: New technologies to monitor the Earth Critical Zone in water-limited ecosystems, funded by Italy-Israel Scientific and Technological Cooperation Programme and from the Interreg VI-A Italy-Slovenia project: WABIN (ITA-SI0600155). BM was supported by the research project EO4WUE Ref. TED2021-129814B-I00, funded by MCIN/AEI (10.13039/501100011033) and the European Union's NextGenerationEU/PRTR, as well as the grant 'RyC2023-045040-I', funded by MICIU/AEI (10.13039/501100011033) and the FSE. Schlingmeier Quarzsand is gratefully thanked for providing sand samples used in this study.

**Author contributions:** Conceptualization GC, NS, MG; Investigation VI, LP; Data curation VI, BM; Formal analysis BM, VI; Visualization VI, BM; Writing—original draft VI; Writing—reviewing and editing VI, BM, LP, GC, NS; Supervision GC.

## SUPPORTING INFORMATION

Supplementary data are available at *GJIRAS* online.

**Figure S1.** Tap water test of the equipment setup to exclude electrode polarization: the resulting phase values remain under 1.5 mrad, (in contrast with the interpreted phase values in the 5–50 mrad range).

**Figure S2.** Example of the Cole–Cole model fitting procedure on the sample with 2 per cent clay content, a pore fluid conductivity of 0.7 S $m^{-1}$ and saturation of 27 per cent. The red dots represent the measured data, the green line the fitted response and the dashed lines the individual Cole–Cole terms. A double Cole–Cole model was applied to account for electromagnetic noise at high frequencies caused by capacitive effects. The high-frequency component was subtracted from the data in order to analyse only the component linked to the true SIP response. The top panel shows the magnitude of the resistivity modulus as a function of frequency, the middle panel presents the phase response, while the bottom panel illustrates the absolute phase residuals between the measured and modelled data. The close agreement between the data and the fitted curves, as well as the low RMS values indicate an excellent fit.

Please note: Oxford University Press is not responsible for the content or functionality of any supporting materials supplied by the authors. Any queries (other than missing material) should be directed to the corresponding author for the paper.

## DATA AVAILABILITY

The data associated with this study are available in the Zenodo data repository: https://doi.org/10.5281/zenodo.18270565

## REFERENCES

Archie, G.E., 1942. The electrical resistivity log as an aid in determining some reservoir characteristics, *Trans.AIME,* **146,** 54–62.

Binley, A. & Slater, L., 2020. *Resistivity and Induced Polarization: Theory and Applications to the Near-Surface Earth,* Cambridge Univ. Press.

Binley, A., Slater, L.D., Fukes, M. & Cassiani, G., 2005. Relationship between spectral induced polarization and hydraulic properties of saturated and unsaturated sandstone: SANDSTONE SIP-HYDRAULIC RELATIONSHIPS, *Water Resour. Res.,* **41**. doi:10.1029/2005WR004202.

Breede, K., Kemna, A., Esser, O., Zimmermann, E., Vereecken, H. & Huisman, J.A., 2012. Spectral induced polarization measurements on variably saturated sand-clay mixtures, *Near Surf. Geophys.,* **10,** 479–489.

Cassiani, G., Kemna, A., Villa, A. & Zimmermann, E., 2009. Spectral induced polarization for the characterization of free-phase hydrocarbon contamination of sediments with low clay content, *Near Surf. Geophys.,* **7,** 547–562.

Cole, K.S. & Cole, R.H., 1941. Dispersion and absorption in dielectrics I. Alternating current characteristics, *J. Chem. Phys.,* **9,** 341–351.

Grunat, D.A., 2013. *Effects of Soil Saturation and Pore Fluid Salinity on Complex Conductivity,* PhD Thesis, Rutgers University-Graduate School-Newark.

Jougnot, D., Ghorbani, A., Revil, A., Leroy, P. & Cosenza, P., 2010. Spectral induced polarization of partially saturated clay-rocks: a mechanistic approach, *Geophys. J. Int.,* **180,** 210–224.

Kemna, A. *et al.*, 2012. An overview of the spectral induced polarization method for near-surface applications, *Near Surf. Geophys.,* **10,** 453–468.

Kemna, A., Binley, A., Ramirez, A. & Daily, W., 2000. Complex resistivity tomography for environmental applications, *Chem. Eng. J.,* **77,** 11–18.

Kessouri, P. *et al.*, 2019. Induced polarization applied to biogeophysics: recent advances and future prospects, *Near Surf. Geophys.,* **17,** 595–621.

Kremer, T., Schmutz, M., Leroy, P., Agrinier, P. & Maineult, A., 2016. Modelling the spectral induced polarization response of water-saturated sands in the intermediate frequency range ($10^2$ –$10^5$ Hz) using mechanistic and empirical approaches, *Geophys. J. Int.,* **207,** 1303–1312.

Leroy, P., Maineult, A., Mendieta, A. & Jougnot, D., 2024. A mechanistic model for the complex conductivity of clay materials. I. Theory, *Geophys. J. Int.,* **241,** 86. doi:10.1093/gji/ggae411.

Lesmes, D.P. & Friedman, S.P., 2005. Relationships between the electrical and hydrogeological properties of rocks and soils, in *Hydrogeophysics Water Science and Technology Library,* pp. 87–128, eds. Rubin, Y. & Hubbard, S.S., Springer.

Lesmes, D.P. & Frye, K.M., 2001. Influence of pore fluid chemistry on the complex conductivity and induced polarization responses of Berea sandstone, *J. geophys. Res.,* **106,** 4079–4090.

Lesmes, D.P. & Morgan, F.D., 2001. Dielectric spectroscopy of sedimentary rocks, *J. geophys. Res.,* **106,** 13329–13346.

Mendieta, A., Jougnot, D., Leroy, P. & Maineult, A., 2021. Spectral induced polarization characterization of non-consolidated clays for varying salinities—an experimental study, *J. geophys. Res. Solid Earth,* **126**. doi:10.1029/2020JB021125.

Okay, G., Leroy, P., Ghorbani, A., Cosenza, P., Camerlynck, C., Cabrera, J. & Florsch, N., 2014. Spectral induced polarization of clay-sand mixtures: experiments and modeling, *Geophysics,* **79,** E353–E375.

Osterman, G., Sugand, M., Keating, K., Binley, A. & Slater, L., 2019. Effect of clay content and distribution on hydraulic and geophysical properties of synthetic sand-clay mixtures, *Geophysics,* **84,** E239–E253.

Pelton, W.H., Ward, S.H., Hallof, P.G., Sill, W.R. & Nelson, P.H., 1978. Mineral discrimination and removal of inductive coupling with multifrequency IP, *Geophysics,* **43,** 588–609.

Peruzzo, L., Schmutz, M., Franceschi, M., Wu, Y. & Hubbard, S.S., 2018. The relative importance of saturated silica sand interfacial and pore fluid geochemistry on the spectral induced polarization response, *J. geophys. Res.: Biogeosciences,* **123,** 1702–1718.

Revil, A., Ghorbani, A., Jougnot, D. & Yven, B., 2023. Induced polarization of clay-rich materials—Part 1: the effect of desiccation, *Geophysics,* **88,** MR195–MR210.

Revil, A., Karaoulis, M., Johnson, T. & Kemna, A., 2012. Review: some low-frequency electrical methods for subsurface characterization and monitoring in hydrogeology, *Hydrogeol J,* **20,** 617–658.

Revil, A. & Skold, M., 2011. Salinity dependence of spectral induced polarization in sands and sandstones: salinity dependence of induced polarization, *Geophys. J. Int.,* **187,** 813–824.

Slater, L., 2007. Near surface electrical characterization of hydraulic conductivity: from petrophysical properties to aquifer geometries—a review, *Surv. Geophys.,* **28,** 169–197.

Slater, L. & Lesmes, D.P., 2002. Electrical-hydraulic relationships observed for unconsolidated sediments: electrical-hydraulic relationships, *Water Resour. Res.,* **38,** 31–31-31-13.

Titov, K., Kemna, A., Tarasov, A. & Vereecken, H., 2004. Induced polarization of unsaturated sands determined through time domain measurements, *Vadose Zone J.,* **3,** 1160–1168.

Ulrich, C. & Slater, L., 2004. Induced polarization measurements on unsaturated, unconsolidated sands, *Geophysics,* **69,** 762–771.

Vanhala, H., 1997. Mapping oil-contaminated sand and till with the Spectral Induced Polarization (SIP) method, *Geophys. Prospect.,* **45,** 303–326.

Vinegar, H.J. & Waxman, M.H., 1984. Induced polarization of shaly sands, *Geophysics,* **49,** 1267–1287.

Weigand, M., 2017. Time-lapse Cole-Cole decomposition routines. Retrieved fromhttps://m-weigand.github.io/ccd_tools/doc_ccd/index.html.

Weigand, M. & Kemna, A., 2016. Debye decomposition of time-lapse spectral induced polarisation data, *Comput. Geosci.,* **86,** 34–45.

Weller, A. & Slater, L., 2012. Salinity dependence of complex conductivity of unconsolidated and consolidated materials: comparisons with electrical double layer models, *Geophysics,* **77,** D185–D198.

Wu, Y. & Peruzzo, L., 2020. Effects of salinity and pH on the spectral induced polarization signals of graphite particles, *Geophys. J. Int.,* **221,** 1532–1541.

Wunderlich, T., Petersen, H., Attia Al Hagrey, S. & Rabbel, W., 2013. Pedophysical Models for Resistivity and Permittivity of Partially Water-Saturated Soils, *Vadose Zone J.,* **12,** 1. doi:10.2136/vzj2013.01.0023.

Zimmermann, E., Kemna, A., Berwix, J., Glaas, W., Münch, H.M. & Huisman, J.A., 2008. A high-accuracy impedance spectrometer for measuring sediments with low polarizability, *Meas. Sci. Technol.,* **19,** 105603. doi:10.1088/0957-0233/19/10/105603.